Numerical Analysis of Quantum Mechanical ∇B Drift*)

Shun-ichi OIKAWA, Takahiro SHIMAZAKI and Emi OKUBO

Faculty of Engineering, Hokkaido University, N-13, W-8, Sapporo 060-8628, Japan

(Received 6 December 2010 / Accepted 1 April 2011)

We have solved the two-dimensional time-dependent Schrödinger equation for a single particle in the presence of a nonuniform magnetic field for initial speeds of 10-100 m/s. By linear extrapolation, it is shown that the variance, or the uncertainty, in position would reach the square of the interparticle separation $n^{-2/3}$ with a number density of $n = 10^{20}$ m^{-3} in a time interval of the order of 10^{-4} sec. After this time the wavefunctions of neighboring particles would overlap, as a result the conventional classical analysis may lose its validity: Plasmas may behave more-or-less like extremely-low-density liquids, not gases, since the size of each particle is of the same order of the interparticle separation.

© *2011 The Japan Society of Plasma Science and Nuclear Fusion Research*

Keywords: grad-B drift, magnetic length, Landau state, quantum mechanical scattering, plasma, diffusion, expansion time

DOI: 10.1585/pfr.6.2401058

1. Introduction

We have solved the two-dimensional time-dependent Schödinger equation for a particle with and without the interparticle potential in a fusion plasma [1], and similar analysis was made with a semi-classical diffusion model [2]. It was shown in such analyses, especially in Ref. [1], that spatial extent of a free particle grows monotonically in time. Such expansion leads to a spatial extent or size of a proton of the order of the average interparticle separation $\Delta\ell \equiv n^{-1/3} \sim 2 \times 10^{-7}$ m in a time interval of $10^6 \times \Delta\ell/v_{\rm th} \sim 10^{-7}$ sec for a plasma with a density $n \sim 10^{20}$ m^{-3} and a temperature $T = mv_{\rm th}^2/2 \sim 10$ keV. It was also shown that, under a Coulomb potential, the wavefunction of a charged particle first shrink and expand in time. In the expansion phase, at times $t \geq 10^{-10}$ sec, the size of particle in the presence of a Coulomb potential is much larger than that in the absence of it.

In analyses by the authors mentioned above, however, the magnetic field $\boldsymbol{B}$ was not explicitly taken into account. The magnetic length $\ell_B \equiv \sqrt{\hbar/qB}$ [3] was introduced only as the initial condition for the time-dependent Schrödinger equation. In this paper, the time-dependent Schrödinger equation will be solved for the ∇B-drift case to find the expansion times in position and in momentum. It is noted that the $\boldsymbol{E} \times \boldsymbol{B}$ case was also analyzed in Ref. [4].

2. Schrödinger Equation

The unsteady Schrödinger equation for wavefunction $\psi(\boldsymbol{r}, t)$, at a position $\boldsymbol{r}$ and a time t, is given by

$$\mathrm{i}\hbar\frac{\partial\psi}{\partial t} = \left[\frac{1}{2m}\Big(-\mathrm{i}\hbar\nabla - q\boldsymbol{A}(\boldsymbol{r})\Big)^2 + q\varphi\right]\psi, \qquad (1)$$

where φ and $\boldsymbol{A}$ stands for the scalar and vector potentials, m and q the mass and electric charge of the particle under consideration, $\mathrm{i} \equiv \sqrt{-1}$ the imaginary unit, and $\hbar \equiv h/2\pi$ the reduced Planck constant. When the corresponding classical particle has an initial momentum $\boldsymbol{p}_0 = m\boldsymbol{v}_0$ at a position $\boldsymbol{r} = \boldsymbol{r}_0$, the initial condition for the wavefunction is given by

$$\psi(\boldsymbol{r}, 0) = \frac{1}{\sqrt{\pi}\sigma_0}\exp\left[-\frac{(\boldsymbol{r}-\boldsymbol{r}_0)^2}{2\sigma_0^2} + \mathrm{i}\boldsymbol{k}_0\cdot\boldsymbol{r}\right], \qquad (2)$$

where $\boldsymbol{r}_0$ is the initial center of ψ, σ_0 is the initial standard deviation, and $\boldsymbol{k}_0 = m\boldsymbol{v}_0/\hbar$ is the initial wavenumber vector.

2.1 Approximation methods

We will solve Eqs. (1) and (2) using the finite difference method in space with the Crank-Nicolson scheme [5]

$$\left(\mathsf{I} - \frac{\Delta t}{2\mathrm{i}\hbar}\mathsf{H}\right)\{\psi^{n+1}\} = \left(\mathsf{I} + \frac{\Delta t}{2\mathrm{i}\hbar}\mathsf{H}\right)\{\psi^n\}, \qquad (3)$$

where I is a unit matrix, H the numerical Hamiltonian matrix, and $\{\psi^n\}$ stands for the discretized set of the two-dimensional time-dependent wavefunction $\psi(x, y, t)$ at a discrete time $t_n = n\Delta t$ to be solved numerically.

We will adopt the successive over relaxation (SOR) scheme for time integration in Eq. (3). The SOR iteration is implemented on a GPU (Nvidia GTX-480: 480 cores @1.40 GHz) [6]. The corresponding classical equation of motion will also be solved in order to check the validity of the numerical results.

2.2 Restriction on the grid spacing

In the numerical analysis of one-dimensional Schrödinger equation for a free particle, the initial momentum is given, using a *one-dimensional* version of

author's e-mail: oikawa@qe.eng.hokudai.ac.jp

*) This article is based on the presentation at the 20th International Toki Conference (ITC20).

© 2011 The Japan Society of Plasma Science and Nuclear Fusion Research

Eq. (2), as

$$\langle p_0 \rangle = \hbar k_0 \sum_{i=-\infty}^{\infty} \frac{\sin k_0 \Delta x}{k_0 \Delta x} |\psi_i|^2 \, \Delta x, \tag{4}$$

which becomes $\hbar k_0$ in the limit of $\Delta x \to 0$, i.e., $\sin k_0 \Delta x \to k_0 \Delta x$. Therefore, the size of spatial discretization for the *two-dimensional* FDM in (x, y) plane should be sufficiently small to satisfy

$$\Delta x \sim \Delta y \ll 1/k_0 = \lambda_0 / 2\pi, \tag{5}$$

where λ_0 is the de Broglie wavelength. This restriction Eq. (5) on Δx and Δy demands a lot of computer memory for fast particles.

The analysis of the two-dimensional time-dependent Schrödinger equation in the presence of a uniform magnetic field [5] showed that the numerical errors are dictated by the grid spacing Δx $(= \Delta y)$ when time-step size Δt satisfies the condition

$$\Delta t \lesssim 0.3 \times (m/\hbar) \times (\Delta x)^2 \ \text{[sec]}, \tag{6}$$

where the factor 0.3 is found numerically [5]. It should be noted that Eq. (6) is not a stability criterion for Δt, since the Crank-Nicolson scheme is unconditionally stable. Instead, we will always choose Δt satisfying Eq. (6) to ensure the numerical errors being a function of $\Delta x = \Delta y$.

2.3 Exact wavefunction in a uniform B field

When the electric field is zero, i.e. $\varphi = \text{const}$, the exact solution $\psi(\boldsymbol{r}, t)$ to Eq. (1), in the case of uniform magnetic field with a Landau gauge [3], $\boldsymbol{A} = (-By, 0, 0)$, is given by

$$\psi(\boldsymbol{r}, t) = \frac{\mathrm{e}^{\mathrm{i}kx}}{\sqrt{\sqrt{\pi}\ell_B}} \exp\left[-\frac{1}{2\ell_B^2}\left(y - \frac{u(t)}{\omega}\right)^2\right] \times \exp\left[\mathrm{i}\left(\frac{y_0^2 \sin 2\omega t}{4\ell_B^2} - \frac{y y_0 \sin \omega t}{\ell_B^2} - \frac{\omega t}{2}\right)\right], \tag{7}$$

where $\ell_B \equiv \sqrt{\hbar/qB}$ is the magnetic length [3], $\omega \equiv qB/m$ the cyclotron frequency, $y_0 \equiv k\ell_B^2$, and $u(t)$ stands for the x-component of the classical velocity of the particle, i.e. $\dot{x}(t) = u(t)$. The y-dependence of $\psi(\boldsymbol{r}, t)$ is essentially the same as that of a one-dimensional harmonic oscillator with the center of the force at $y = -y_0$. It is apparent in Eq. (7) that the standard deviation, or uncertainty, in position does not change in time; $\sigma_r^2(t) = \ell_B^2 = \text{const}$.

3. Quantum Mechanical ∇B Motion

Now, let the electrostatic potential $\varphi = \text{const}$. and the vector potential be

$$\boldsymbol{A} = (-y(1 - y/2L_B)\, B, 0, 0), \tag{8}$$

where L_B represents the gradient length scale for the magnetic field. The corresponding classical motion is called the grad-B drift along x-axis. We will solve the time-dependent Schrödinger equation given in Eq. (1) with the Coulomb gauge given in Eq. (8), for several cyclotron periods.

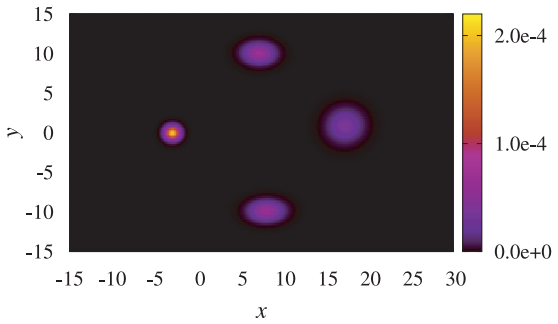

Fig. 1 Time evolution of the probability density function (PDF), $\psi^*\psi$ at the normalized times ωt of $0, \pi/2, \pi$, and $3\pi/2$ in the normalized x-y plane. The smallest circle on the left represents the initial PDF at a time $\omega t = 0$, and it rotates clockwise.

The numerical results to be presented in the following sections are normalized by the cyclotron radius of a proton for $B = 10$ T with $v_0 = 10$ m/s. The normalized system size is $-50 \le x, y \le 50$. The normalized spatial grid-sizes are $\Delta x = \Delta y = 0.02$, and the normalized time-step is $\Delta t = 2\pi \times 10^{-5}$, which corresponds to the numerical factor of 0.05 instead of 0.3 appeared in Eq. (6) for Δt. The normalized length scale is $L_B = 5 \times 10^8$, dimensional value of which is 5.219 m. We judge the convergence in the SOR scheme being reached when $\left|r_{i,j}\right|^2 < 10^{-32}$, where $r_{i,j}$ is the complex residual of Eq. (3) at each grid point (x_i, y_j).

Figure 1 shows the time evolution of the probability density function (PDF), $\psi^*\psi$, for an initial particle speed of $v_0 = 100$ m/s at the normalized times ωt of $0, \pi/2, \pi$, and $3\pi/2$ in the normalized x-y plane. In this figure, the smallest and brightest circle on the left represents the initial PDF at a time $\omega t = 0$, and it rotates clockwise. It is noted that the shape of the PDF are circle at the normalized time of $\omega t = 0$ and π, whereas they are ellipse when $\omega t = \pi/2$ and $3\pi/2$, because of the distribution of vector potential $\boldsymbol{A} = \boldsymbol{A}(y)$.

Figure 2 compares the guiding-center position $\boldsymbol{r}_\mathrm{G}$ in the normalized x-y plane between the classical orbit $\boldsymbol{r}_\mathrm{G}(t)$ and the quantum-mechanical expectation $\langle \boldsymbol{r}_\mathrm{G} \rangle$, which is defined as

$$\langle \boldsymbol{r}_\mathrm{G} \rangle = \int_\Sigma \psi^*(\boldsymbol{r}, t) \left(\boldsymbol{r} + \boldsymbol{v} \times \boldsymbol{\omega}/\omega^2\right) \psi(\boldsymbol{r}, t) \, \mathrm{d}^2 \boldsymbol{r}, \tag{9}$$

in the normalized x-y plane Σ. Here $\boldsymbol{\omega} = q\boldsymbol{B}/m$ is the cyclotron frequency vector, and the operator $\boldsymbol{v}$ is

$$m\boldsymbol{v} = -\mathrm{i}\hbar\nabla - q\boldsymbol{A}. \tag{10}$$

The amplitude of $\langle y_\mathrm{G} \rangle$ is smaller than $y_\mathrm{G}(t)$ due to the finite grid size, however, the ∇B drift along x-direction is in good agreement.

Figure 3 shows the time evolution of the variances in

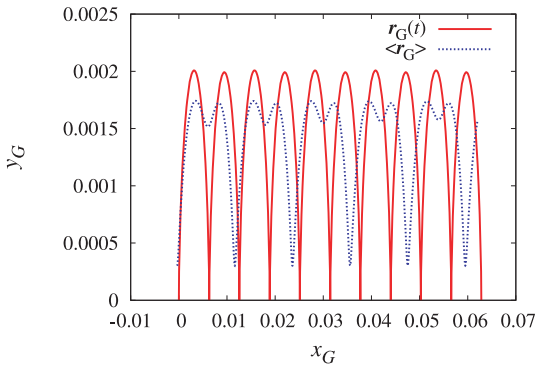

Fig. 2 Comparison of the guiding-center position $\boldsymbol{r}_{\mathrm{G}}$ in the normalized x-y plane: the quantum-mechanical expectation $\langle \boldsymbol{r}_{\mathrm{G}} \rangle$ and the classical orbit $\boldsymbol{r}_{\mathrm{G}}(t)$ with $\boldsymbol{r}_{\mathrm{G}}(0) = 0$.

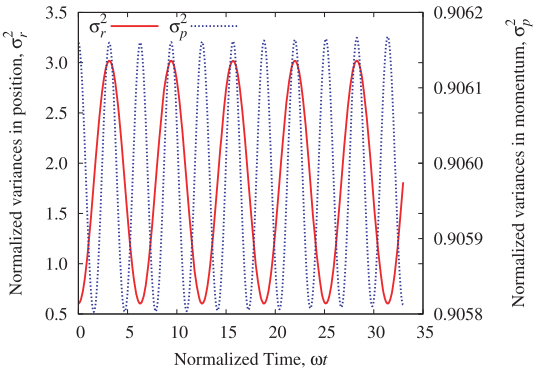

Fig. 3 Normalized variances σ_r^2 and σ_p^2 vs. normalized time ωt for $v_0 = 10$ m/s and $L_B = 5.219$ m; σ_r^2 in position, and σ_p^2 in momentum.

position and in mechanical momentum for $v_0 = 10$ m/s, respectively, which are defined as

$$\sigma_r^2 = \int_\Sigma \psi^* \left(\boldsymbol{r} - \langle \boldsymbol{r} \rangle\right)^2 \psi \, \mathrm{d}^2\boldsymbol{r}, \tag{11}$$

$$\sigma_p^2 = \int_\Sigma \psi^* \left(-\mathrm{i}\hbar\nabla - q\boldsymbol{A} - \langle \boldsymbol{p} \rangle\right)^2 \psi \, \mathrm{d}^2\boldsymbol{r}, \tag{12}$$

where $\langle \boldsymbol{p} \rangle$ is the expectation value of the mechanical momentum:

$$\langle \boldsymbol{p} \rangle = \int_\Sigma \psi^* \left(-\mathrm{i}\hbar\nabla - q\boldsymbol{A}\right) \psi \, \mathrm{d}^2\boldsymbol{r}. \tag{13}$$

These variances oscillate with the cyclotron period in position and with half the cyclotron period in mechanical momentum. It should be noted that their peaks grow in time.

Figures 4 and 5, respectively show the grid size and the timestep dependence of the increment of peak variance. The normalized grid size of $\Delta x = \Delta y \lesssim 0.1$ is sufficiently small to use. Thus we have used $\Delta x = \Delta y = 0.02$ and $\Delta t = 2\pi \times 10^{-5}$ throughout the calculation. As for the numerical errors in variance, it is noted in Ref. [1] that our code is capable of accurately reproducing the time-dependent variance in position $\sigma_r^2(t)$ for a free particle, for which an exact solution is available.

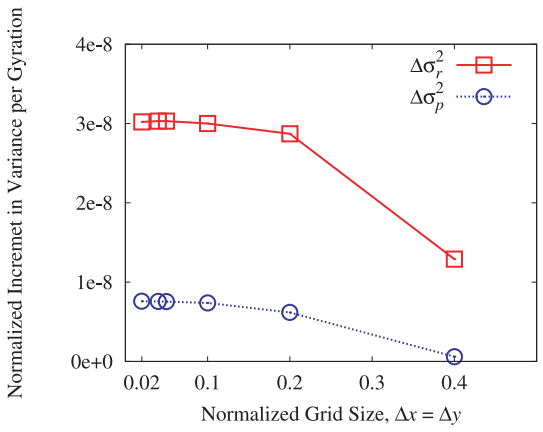

Fig. 4 Normalized incremental variances per gyration vs. normalized grid spacing $\Delta x = \Delta y$ with $\Delta t = 2\pi \times 10^{-5}$. Other parameters are the same as those in Fig. 3.

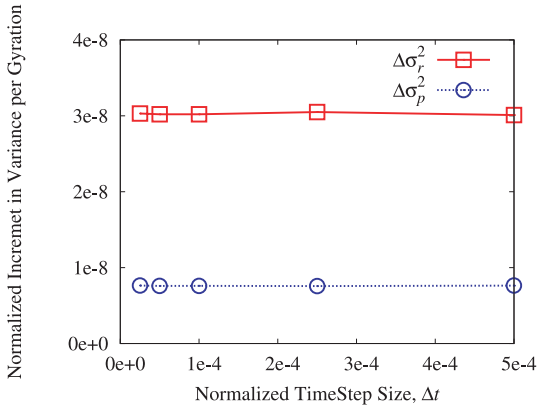

Fig. 5 Normalized incremental variances per gyration vs. normalized grid spacing Δt with $\Delta x = \Delta y = 0.02$. Both vaiances converge for $\Delta t \lesssim 5 \times 10^{-4}$. Other parameters are the same as those in Fig. 3.

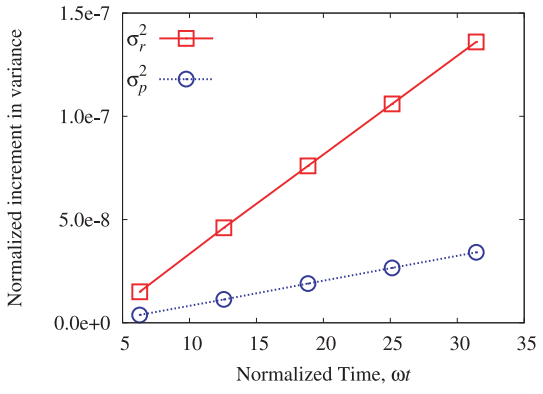

Fig. 6 Normalized increment of peak variance σ_r^2 in position with red squares and σ_p^2 in momentum with blue circles for $v_0 = 10$ m/s with $L_B = 5.219$ m.

Figure 6 shows the increments, due to nonuniformity of the magnetic field, of peaks of the variances in position and in momentum, respectively. Both increments in position and momentum are in proportion to the time t. This

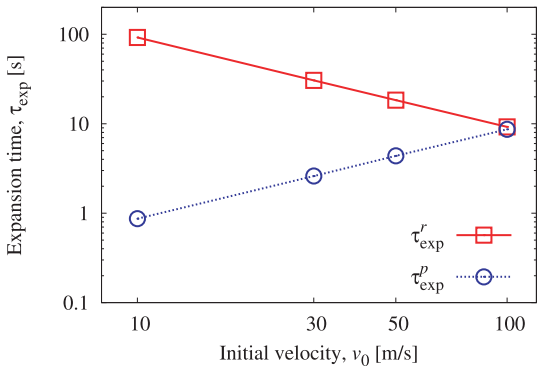

Fig. 7 Initial speed v_0 dependence of the expansion times in position τ^r_{exp} and in mechanical momentum τ^p_{exp} in sec, for $L_B = 5.219$ m, the normalized timestep of $\Delta t = 2\pi\times10^{-5}$, and the normalized grid size of $\Delta x = \Delta y = 0.02$.

means that the variances would reach some critical values as time goes, such as the square of the interparticle separation for variances in position, and the square of the thermal speed for variance in velocity (or momentum).

Let us define the *expansion time* in position τ^r_{exp} and in mechanical momentum τ^p_{exp}, respectively, as

$$\tau^r_{exp} \equiv \frac{(\Delta\ell)^2}{\Delta\sigma_r^2} T_c, \tag{14}$$

$$\tau^p_{exp} \equiv \frac{(mv_0)^2}{\Delta\sigma_p^2} T_c, \tag{15}$$

where $\Delta\sigma_r^2$ and $\Delta\sigma_p^2$ represent the increments of the variance in position and in mechanical momentum, respectively, per cyclotron period $T_c = 2\pi/\omega$.

The red squares in Fig. 7 represent the initial speed dependence of the expansion time τ^r_{exp}, during which the variance in position reaches the square of interparticle separation $(\Delta\ell)^2 \equiv n^{-2/3}$ with the number density of $n = 10^{20}$ m^{-3} for various initial speeds of $v_0 = 10, 30, 50$ and 100 m/s. If the particle is in a typical fusion plasma with such a number density, the variance in position would reach the square of the interparticle separation $n^{-2/3}$m^2 for $v_0 = 10^6$ m/s by linear extrapolation $\tau^r_{exp} = \tau^r_{exp}(v_0)$, in a time interval of 2×10^{-4} sec. After this time the conventional classical analyses, especially on diffusion, may be invalid: plasmas may behave more-or-less like extremely-low-density liquids, not gases, since the size of each particle is the same as the interparticle separation, accordingly the neighboring wavefunctions overlap.

Also depicted with blue circles in Fig. 7 are the expansion time in mechanical momentum τ^p_{exp}, during which the variance in mechanical momentum reaches the square of its initial momentum, $(mv_0)^2$. The classical counterpart of the expansion time in momentum τ^p_{exp} is the momentum transfer time, or the deflection time τ_d. Thus, if $\tau^p_{exp} \ll \tau_d$, the expansion in momentum could make *collision* frequency and cross-section much larger than that with classical theories [7–9]. By linear extrapolation, however, the expansion time in momentum would be of the order of 10^4 sec for $v_0 \sim 10^6$ m/s, and is of little interest for fast particles.

4. Summary and Discussion

We have solved the two-dimensional time-dependent Schödinger equation for a single particle in the presence of a nonuniform magnetic field. It is shown that the variance, or the uncertainty, in position would reach the square of the interparticle separation $\Delta\ell$ for $v_0 = 10^6$ m/s and $n = 10^{20}$ m^{-3} in a time interval of 2×10^{-4} sec. After this time the conventional classical analysis may be invalid.

In real plasmas, since charged particles suffer fluctuations of microscopic electrostatic potentials due to other particles, deviations could grow much faster.

The expansion time of $\tau^r_{exp} \sim 10^{-4}$ sec estimated in this study is obtained from numerical calculations for a single charged particle during a short time interval of $\sim10^{-7}$ sec by using linear extrapolation. Several many-body effects may reduce or enhance the quantum-mechanical expansion, such as the potential screening by electrons and/or interparticle Coulomb force. Such studies will be left for future work.

Acknowledgments

The authors would like to thank Prof. Y. Matsumoto, and Prof. M. Itagaki for their fruitful discussions on the subject. Part of the SOR coding with GPU was done by Mr. R. Ueda. This research was partially supported by a Grant-in-Aid for Scientific Research (C), 21560061.

[1] S. Oikawa, T. Oiwa and T. Shimazaki, Plasma Fusion Res. **5**, S2024 (2010).
[2] S. Oikawa, T. Shimazaki and T. Oiwa, Plasma Fusion Res. **5**, S2025 (2010).
[3] L.D. Landau and E.M. Lifshitz, *Quantum Mechanics*: *Non-relativistic Theory*, 3rd ed., translated from the Russian by J.B. Sykes and J.S. Bell (Pergamon Press, Oxford, 1977).
[4] S. Oikawa, T. Shimazaki and E. Okubo, ITC20, P1-93 (2010).
[5] H. Natori and T. Munehisa, J. Phys. Soc. Jpn. **66**, 351 (1997).
[6] http://www.nvidia.com.
[7] R.S. Cohen, L. Spitzer, Jr. and P.McR. Routly, Phys. Rev. **80**, 230 (1950).
[8] S.I. Braginskii, *Reviews of Plasma Physics*, M.A. Leontovich (ed.), (Consultants Bureau, New York, 1965).
[9] R.J. Hawryluk, Rev. Mod. Phys. **70**, 537 (1998).